Bulk and surface plasmon polariton excitation in RuO_2 for low-loss plasmonic applications in NIR

L. Wang,[1,*] C. Clavero,[2] K. Yang,[2] E. Radue,[1] M. T. Simons,[1] I. Novikova,[1] and R. A. Lukaszew[1,2]

[1]*Department of Physics, College of William & Mary, Williamsburg, VA 23187, USA*
[2]*Department of Applied Science, College of William and Mary, Williamsburg, VA 23187, USA*
**lwang02@email.wm.edu*

Abstract: Transition-metal oxides, such as RuO_2, offer an exciting alternative to conventional metals for metamaterials and plasmonic applications due to their low optical losses in the visible and near-infrared ranges. In this manuscript we report observation of optically excited surface plasmon polaritons (SPPs) and bulk plasmons in RuO_2 thin films grown using DC reactive magnetron sputtering on glass and TiO_2 (001) substrates. We show that both plasmon modes can exist simultaneously for the infrared region of the optical spectrum, while only the bulk plasmons are supported at higher optical frequencies. Finally, we demonstrate that the film properties can be tailored to favor excitation of either SPP or bulk plasmons.

OCIS codes: (240.6680) Surface plasmons; (310.0310) Thin films; (250.5403) Plasmonics.

References and links

1. L. Dominici, F. Michelotti, T. M. Brown, A. Reale, and A. Di Carlo, "Plasmon polaritons in the near infrared on fluorine doped tin oxide films," Opt. Express **17**(12), 10155–10167 (2009).
2. K. Welford, "Surface plasmon-polaritons and their uses," Opt. Quantum Electron. **23**(1), 1–27 (1991).
3. J. Biener, G. W. Nyce, A. M. Hodge, M. M. Biener, A. V. Hamza, and S. A. Maier, "Nanoporous plasmonic metamaterials," Adv. Mater. (Deerfield Beach Fla.) **20**(6), 1211–1217 (2008).
4. N. Engheta, "Circuits with light at nanoscales: optical nanocircuits inspired by metamaterials," Science **317**(5845), 1698–1702 (2007).
5. G. X. Li, Z. L. Wang, S. M. Chen, and K. W. Cheah, "Narrowband plasmonic excitation on gold hole-array nanostructures observed using spectroscopic ellipsometer," Opt. Express **19**, 6356–6361 (2011).
6. Y. W. Cao, R. Jin, and C. A. Mirkin, "DNA-modified core-shell Ag/Au nanoparticles," J. Am. Chem. Soc. **123**(32), 7961–7962 (2001).
7. R. Pratibha, K. Park, I. I. Smalyukh, and W. Park, "Tunable optical metamaterial based on liquid crystal-gold nanosphere composite," Opt. Express **17**(22), 19459–19469 (2009).
8. I. H. El-Sayed, X. H. Huang, and M. A. El-Sayed, "Surface plasmon resonance scattering and absorption of anti-EGFR antibody conjugated gold nanoparticles in cancer diagnostics: Applications in oral cancer," Nano Lett. **5**(5), 829–834 (2005).
9. A. Boltasseva and H. A. Atwater, "Materials science. Low-loss plasmonic metamaterials," Science **331**(6015), 290–291 (2011).
10. G. V. Naik, A. Boltasseva; "A comparative study of semiconductor-based plasmonic metamaterials," Metamaterials (Amst.) **5**(1), 1–7 (2011).
11. C. Clavero, K. Yang, J. R. Skuza, and R. A. Lukaszew, "Magnetic field modulation of intense surface plasmon polaritons," Opt. Express **18**(8), 7743–7752 (2010).
12. G. V. Naik, J. Kim, and A. Boltasseva, "Oxides and nitrides as alternative plasmonic materials in the optical range," Opt. Mater. Express **1**(6), 1090–1099 (2011).
13. R. Won, "View from...NANOMETA 2011: In search of new materials," Nat. Photonics **5**(3), 139–140 (2011).
14. R. Ziblat, V. Lirtsman, D. Davidov, and B. Aroeti, "Infrared surface plasmon resonance: A novel tool for real time sensing of variations in living cells," Biophys. J. **90**(7), 2592–2599 (2006).
15. W. DiPippo, B. J. Lee, and K. Park, "Design analysis of doped-silicon surface plasmon resonance immunosensors in mid-infrared range," Opt. Express **18**(18), 19396–19406 (2010).
16. M. Righini, A. S. Zelenina, C. Girard, and R. Quidant, "Parallel and selective trapping in a patterned plasmonic landscape," Nat. Phys. **3**(7), 477–480 (2007).
17. P. F. Robusto and R. Braunstein, "Optical measurements of the surface-plasmon of indium tin oxide," Phys. Status Solidi A **119**(1), 155–168 (1990).
18. C. Rhodes, S. Franzen, J. P. Maria, M. Losego, D. N. Leonard, B. Laughlin, G. Duscher, and S. Weibel, "Surface plasmon resonance in conducting metal oxides," J. Appl. Phys. **100**(5), 054905 (2006).

#162843 - $15.00 USD Received 9 Feb 2012; revised 22 Mar 2012; accepted 23 Mar 2012; published 28 Mar 2012

19. C. Rhodes, M. Cerruti, A. Efremenko, M. Losego, D. E. Aspnes, J. P. Maria, and S. Franzen, "Dependence of plasmon polaritons on the thickness of indium tin oxide thin films," J. Appl. Phys. **103**(9), 093108 (2008).
20. R. B. Pettit, J. Silcox, and R. Vincent, "Measurement of surface-plasmon dispersion in oxidized Aluminum films," Phys. Rev. B **11**(8), 3116–3123 (1975).
21. C. C. Hu, K. H. Chang, M. C. Lin, and Y. T. Wu, "Design and tailoring of the nanotubular arrayed architecture of hydrous RuO_2 for next generation supercapacitors," Nano Lett. **6**(12), 2690–2695 (2006).
22. L. F. Mattheiss, "Electronic structure of RuO_2, OsO_2, and IrO_2," Phys. Rev. B **13**(6), 2433–2450 (1976).
23. K. Glassford and J. Chelikowsky, "Electron transport properties in RuO_2 rutile," Phys. Rev. B **49**(11), 7107–7114 (1994).
24. P. Hones, T. Gerfin, and M. Gratzel, "Spectroscopic ellipsometry of RuO_2 films prepared by metalorganic chemical vapor deposition," Appl. Phys. Lett. **67**(21), 3078–3080 (1995).
25. D. Búc, M. Mikula, D. Music, U. Helmersson, P. Jin, S. Nakao, K. Y. Li, P. W. Shum, Z. Zhou, and M. Čaplovičová, "Ruthenium oxide films prepared by reactive unbalanced magnetron sputtering," J. Electric. Eng. **55**, 39–42 (2004).
26. E. Kretschmann and H. Raether, "Radiative decay of nonradiative surface plasmon excited by light," Z. Naturforsch. **23a**, 2135–2136 (1968).
27. H. S. Nalwa, *Handbook of Thin Film Materials: Semiconductor and Superconductor Thin Films* (Academic, 2002).
28. S. K. Hong, H. J. Kim, and H. G. Yang, "Stress measurements of radio-frequency reactively sputtered RuO_2 thin films," J. Appl. Phys. **80**(2), 822–826 (1996).
29. J. H. Huang and J. S. Chen, "Material characteristics and electrical property of reactively sputtered RuO_2 thin films," Thin Solid Films **382**(1-2), 139–145 (2001).
30. A. K. Goel, G. Skorinko, and F. H. Pollak, "Optical properties of single-crystal rutile RuO_2 and IrO_2 in the range 0.5 to 9.5 eV," Phys. Rev. B **24**(12), 7342–7350 (1981).
31. M. Schubert, "Polarization-dependent optical parameters of arbitrarily anisotropic homogeneous layered systems," Phys. Rev. B **53**(8), 4265–4274 (1996).
32. M. Schubert, T. E. Tiwald, and J. A. Woollam, "Explicit solutions for the optical properties of arbitrary magneto-optic materials in generalized ellipsometry," Appl. Opt. **38**(1), 177–187 (1999).

1. Introduction

Polaritons result from strong coupling between electromagnetic waves and phonons and/or plasmons, which are respectively charge oscillations of ions in a multipolar lattice or just of the charge density [1]. Bulk polaritons are propagating wave modes inside a medium without considering boundary conditions, *i.e.* the medium is considered "infinite". If the wave is bound by a surface with free electrons it is called surface plasmon polariton (SPP) [2]. SPPs have been experimentally and theoretically studied for many years due to their possible use in novel photonic and sensing applications. Conventional metals such as Au and Ag have traditionally been used for metamaterials and other plasmonic applications [3–8]; however, their use is limited by high losses in the visible and near-infrared (NIR) ranges and very large negative real permittivity values [9–11].

Alternative low-loss materials, such as conducting oxide films, are potentially advantageous for many plasmonic applications, since they exhibit both a small negative real permittivity and relatively small losses in the NIR. In general, conducting oxide materials have much lower free charge carrier concentrations ($10^{20\text{-}22} cm^{-3}$) as compared to metals ($>10^{23} cm^{-3}$). This makes their plasma frequencies smaller, and hence their imaginary permittivity and losses lower than those of metals [12], making them suitable for metamaterial devices and transformation optics such as superlenses [10], hyperlenses [13] as well as other applications. In addition, innovative devices can be considered for uses such as increased depth sensing of living cells in the NIR [14, 15] or infrared enhanced trapping for SPP-based tweezer applications [16]. In fact, several researchers are currently considering conducting oxides and nitrides as alternative plasmonic materials, including indium tin oxide (ITO) [17–19], fluorine doped tin oxide (FTO or SFO) [1], aluminum doped zinc oxide (AZO) [20] and some nitrides such as TiN or ZrN [12].

In this manuscript we present an experimental and theoretical investigation of polariton excitation in RuO_2 to evaluate its prospective use as an alternative plasmonic material for the NIR spectral region. RuO_2 belongs to the family of transition-metal dioxide compounds with rutile type structure, and it exhibits metallic conductivity and high thermal and chemical stability [21]. Its band structure has been calculated by Mattheiss [22] and Glassford [23]. RuO_2 has a small plasma frequency of 3.3eV [23, 24], which translates to small losses. The

#162843 - $15.00 USD Received 9 Feb 2012; revised 22 Mar 2012; accepted 23 Mar 2012; published 28 Mar 2012

imaginary part of permittivity of RuO_2 in the visible and NIR regions is comparable to those of other low-loss oxides and nitrides, like ITO, AZO and TiN [12]. Besides, RuO_2 has a small negative real part of permittivity ε' in the infrared (IR) region. This property is essential for transformative optics applications in which similar magnitudes of ε' for the plasmonic and dielectric components are required. In addition, the lower plasma frequency of RuO_2 makes it necessary to consider both bulk plasmons and surface plasmon polaritons when considering optical excitations in the visible and NIR ranges. This distinguishes RuO_2 from normal metals, where large plasma frequencies make bulk polaritons irrelevant in this spectral range.

By performing a complete experimental and theoretical study of bulk polaritons and SPPs in RuO_2 thin films, we demonstrate that both can be observed simultaneously in the IR region, while only bulk polaritons are observed in the visible red region. The co-existence of two plasmon modes opens interesting possibilities for increasing the efficiency of plasmon enhanced photovoltaic devices. At the same time, bulk plasmons must be taken into account as a possible loss mechanism. Our results also suggest that depending on the application, it may be possible to tailor the properties of a RuO_2 film to favor either SPP or bulk plasmon excitation.

2. Experimental approach

RuO_2 thin films were prepared on glass substrates and TiO_2 (001) substrates by DC reactive magnetron sputtering. Films were sputtered at a power of 20 W in Ar + O_2 mixture with Ar partial pressure of 4.00 mTorr and O_2 partial pressure ranging from 0.01 to 0.10 mTorr using a planar round ruthenium target (purity 99.95%). Substrates were annealed at $500\,°C$ for 30 minutes prior growth and held at this temperature during growth since it has been shown to yield high quality thin films [25]. The first series of films (Series I) was deposited on TiO_2 (001) substrates at different O_2 partial pressures ranging from 0.01 to 0.1 mTorr while keeping the same deposition time of 8 minutes (average thickness around 30 nm) in order to investigate the optimal deposition parameters in terms of film crystalline quality and optical properties. The second series (Series II) of films was deposited on TiO_2 (001) substrates using the optimal partial pressure of O_2 found in Series I (0.04 mTorr), while the thickness of the films was varied from 17 to 128 nm in order to investigate how the bulk and SPP modes evolve with thickness. We also deposited a 30 nm RuO_2 film on a glass substrate under the same growth condition of Series II samples to compare substrate effects. The growth rates under different O_2 partial pressures were found nearly the same, around 0.625 Å /s, calculated from X-ray reflectivity (XRR) measurements.

The structure of the films was investigated by reflection high-energy electron diffraction (RHEED) and X-ray diffraction (XRD) techniques. Four-point probe and ellipsometry were used to characterize the transport and optical properties of the films respectively. Ellipsometry measurements were performed in the 1.7-3.0 eV photon energy range using a variable angle spectroscopic ellipsometer.

The optical response of the RuO_2 thin films under plasmon excitation was investigated in the Kretschmann configuration [26] using *p*-polarized lasers, including a He-Ne red laser (λ =632.8 nm), a He-Ne IR laser (λ =1520 nm) and a tunable ultrafast laser (470 nm-2.5 um). In this configuration, the glass substrate or the TiO_2 (001) substrate were attached to a semicylindrical glass prism (n =1.5018) using a refractive index matching oil (n = 1.5018). The sample attached to the prism was mounted on an automated goniometer allowing illumination in total internal reflection with variable incidence angle θ and angle resolution of 10^{-4} degree. The intensity variations were detected by corresponding detectors preceded by a *p*-oriented polarizer.

3. RuO_2 film characterizations

Good characterization of the microstructure and transport properties of thin films is important in order to correlate these with their optical properties. Thus, RHEED images were obtained as evidence for the in-plane microstructure of the RuO_2 thin films. Figure 1 shows the

#162843 - $15.00 USD Received 9 Feb 2012; revised 22 Mar 2012; accepted 23 Mar 2012; published 28 Mar 2012

RHEED patterns for 30 nm RuO_2 thin films deposited on a glass substrate (Fig. 1a) and on a TiO_2 (001) substrate along the TiO_2 [100] (Fig. 1b) and [110] directions (Fig. 1c). As shown in Fig. 1(a), the RHEED image shows rings, indicating a polycrystalline microstructure for RuO_2 deposited on glass substrate, while in Figs. 1(b), 1(c) the RHEED images show clear streaks, which means that the RuO_2 deposited on TiO_2 (001) substrates exhibit good crystalline structure following the epitaxial relation RuO_2[100](001)||TiO_2[100](001). The discontinuous streaks shown in Figs. 1(b), 1(c) are due to three-dimensional growth mode which precludes atomically flat surfaces.

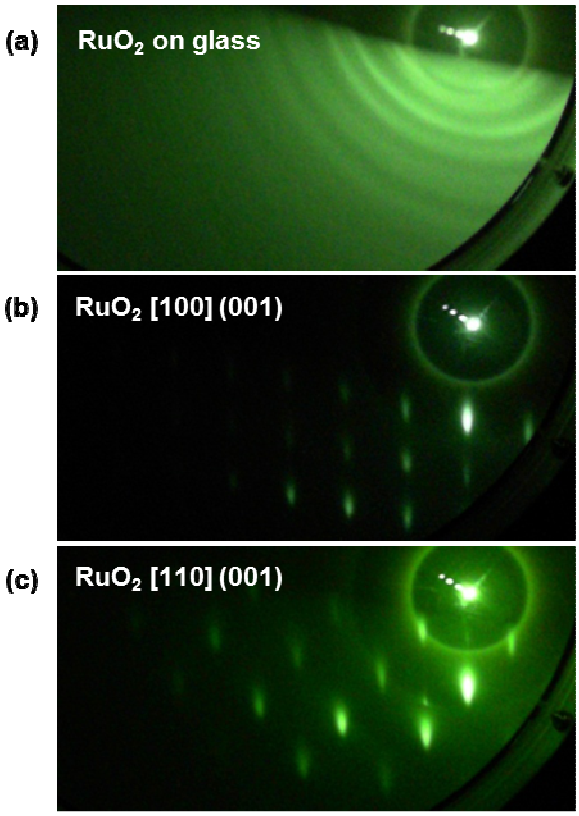

Fig. 1. RHEED images show polycrystalline structure of RuO_2 deposited on glass (a) and single crystalline structure of RuO_2 deposited on a TiO_2 (001) substrate along the TiO_2 [100] direction (b) and [110] direction (c).

Multiple structural and optical characterization techniques were applied to find the optimal O_2 partial pressure during growth in terms of microstructure and optical properties of the RuO_2 films. XRD symmetric scans for Series I are shown in Fig. 2(a). RuO_2 (002) peaks are observed for all the RuO_2 films deposited at different pressures. Nevertheless, the film grown at O_2 partial pressure of 0.04 mTorr shows the RuO_2 (002) peak position nearest to the expected bulk peak value. The average grain size, plane spacing and lattice parameter extracted from XRD data are shown in Table 1. The average grain size is around 180 Å for all the films in this series. Interestingly, the film grown under O_2 partial pressure of 0.04 mTorr shows the smallest lattice parameter mismatch (0.17%) with respect to bulk single crystal RuO_2 with lattice parameter c = 3.1059 Å [27]. The evolution of the lattice parameter as a function of O_2 partial pressure is shown in Fig. 2(b), where the dash line stands for the lattice parameter *c* for bulk single crystal RuO_2 for reference.

The electrical conductivity properties of the RuO_2 films in Series I were investigated by measuring their sheet resistance values using the four-point probe technique. As shown in Fig. 2(b), the RuO_2 thin film grown at O_2 partial pressure of 0.04 mTorr shows the lowest sheet

#162843 - $15.00 USD Received 9 Feb 2012; revised 22 Mar 2012; accepted 23 Mar 2012; published 28 Mar 2012

resistance, around 27.49 Ω/□, which is comparable to other sputtered RuO_2 thin films in previous reports [28, 29]. A correlation between lattice parameter and sheet resistance was found, as shown in Fig. 2(b). We note that when the lattice parameter of the RuO_2 thin film is closest to bulk value (O_2 partial pressure of 0.04 mTorr) the film also exhibits the smallest sheet resistance.

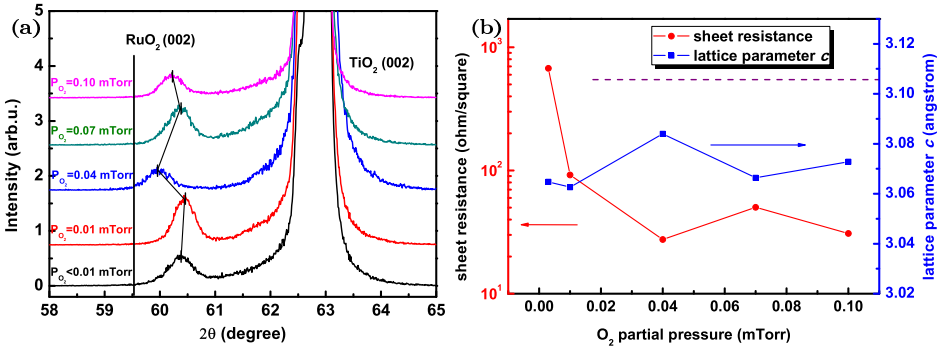

Fig. 2. (a) XRD symmetric scans for Series I samples (RuO_2 deposited on TiO_2 (001) substrates with similar film thickness around 30 nm under different O_2 partial pressure conditions). The continuous vertical line shows the position of the bulk RuO_2 (002) peak. The small connected vertical lines show the RuO_2 (002) peaks positions for the different samples. The film grown at O_2 partial pressure of 0.04 mTorr shows the RuO_2 (002) peak position nearest to the expected bulk peak values. (b) Sheet resistance measured from four-point probe and lattice parameter extracted from XRD data of Series I samples. Dash line stands for the lattice parameter *c* for single crystal RuO_2.

Table 1. Average grain size, planes spacing *d* (002) and lattice parameter *c* of RuO_2 thin films deposited on TiO_2 (001) substrates in Series I from XRD analysis

Series I O_2 partial pressure (mTorr)	Average Grain Size (Å)	*d* (002) (Å)	Lattice Parameter *c* (Å ± 0.001 Å)	Lattice parameter mismatch percent (%) (*c*_bulk = 3.1059 Å)
<0.01	163.17	1.532	3.065	0.33
0.01	197.79	1.531	3.063	0.35
0.04	180.93	1.542	3.084	0.17
0.07	173.56	1.533	3.066	0.32
0.10	181.15	1.536	3.073	0.27

Ellipsometry measurements were performed in the 1.7-3.0 eV photon energy range to characterize the optical properties of the RuO_2 thin films. Measurements were taken at different angles from 45° to 75°. The real and imaginary part of the dielectric constants of the RuO_2 thin films were extracted from the ellipsometry data considering film thickness determined from XRR. Figures 3(a) and 3(b) shows the extracted dielectric function $\varepsilon = \varepsilon' + i\varepsilon''$ of RuO_2 thin films grown at different O_2 partial pressures in Series I. The dielectric functions of single crystal RuO_2 obtained from Ref [30] are included for comparison. From Fig. 3, it is clear that RuO_2 films grown at O_2 partial pressure of 0.04 mTorr, which were previously shown to have the lattice parameter closest to bulk, have also optical constants approaching bulk values. While the real part of the dielectric function is almost identical to bulk, its imaginary part ε'' has higher value. This can be attributed to increased light absorption due to microstructure defects and surface roughness, which have been neglected in the experiments of Goel *et al.* [30] with single crystals.

#162843 - $15.00 USD Received 9 Feb 2012; revised 22 Mar 2012; accepted 23 Mar 2012; published 28 Mar 2012

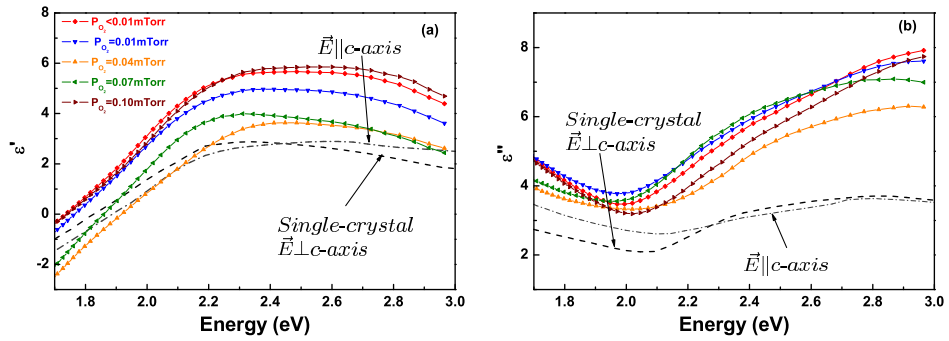

Fig. 3. (a) Real ε' and (b) imaginary ε'' parts of the dielectric function for the RuO_2 thin films deposited on TiO_2 (001) substrates under different O_2 partial pressures in Series I. The dielectric functions of RuO_2 single crystal (Ref. [30]) are included for comparison.

From the characterization procedures described above it was established that films grown at O_2 partial pressure of 0.04 mTorr exhibit optimized crystal structure as well as electrical and optical properties. As a result, a new Series II of RuO_2 thin films were deposited on TiO_2 (001) substrates at O_2 partial pressure of 0.04 mTorr varying the film thicknesses. Details related to the characterization of Series II samples will not be discussed since the reproducibility of the films during the growth process is very high and they were found to have identical properties than the sample grown at O_2 partial pressure of 0.04 mTorr in Series I.

4. Dispersion curves and simulated reflectance map

As a first approximation, it is possible to derive the dispersion curve for the propagating bulk polariton modes inside each of the two media (medium 1 and 2) using their dielectric functions $\varepsilon_{1,2}(E)$:

$$q_{1,2} = \frac{\omega}{c}\sqrt{\varepsilon_{1,2}(E)} \tag{1}$$

and for the propagating modes at the interface, *i.e.* the SPP modes:

$$k = \frac{\omega}{c}\sqrt{\frac{\varepsilon_1(E)\varepsilon_2(E)}{\varepsilon_1(E)+\varepsilon_2(E)}} \tag{2}$$

where q_i (i = 1, 2) is the total wavevector inside the bulk medium i, and k is the in-plane wavevector component at the interface. For our calculations, we used the dielectric function $\varepsilon(E)$ of RuO_2 derived using a classic Drude model with three harmonic oscillators reported in Ref 24. The Drude term describes the contribution of the free carriers, while the harmonic oscillators represent various inter-band transitions. Figure 4(a) shows the dispersion relation curves for bulk and surface modes in RuO_2 in the case of RuO_2/air interface. The requirement for SPPs propagating at the RuO_2/air interface is that $\varepsilon' < -\varepsilon_{air} = -1$ (ε' is the real part of the dielectric function of RuO_2). As a result, the upper frequency limit for SPPs is $\omega_{sp} = \omega(\varepsilon'=-1) = 1.78$eV [24], *i.e.* SPPs in RuO_2 can be excited in the IR region (λ >700 nm). As shown in Fig. 4(a), the surface mode dispersion without considering damping (*i.e.* only considering the real part of the dielectric function) bends below the light line for small momentum and then asymptotically tends to ω_{sp} for larger momentum (dotted line). This mode is often referred to as a Fano mode. Consideration of damping causes a back-bending for both the bulk mode (dashed line) and the SPP dispersion curve (solid line). It is worth

#162843 - $15.00 USD Received 9 Feb 2012; revised 22 Mar 2012; accepted 23 Mar 2012; published 28 Mar 2012

noticing that a complex dielectric function $\varepsilon(E)$ implies q and k are also complex. In Fig. 4(a), k and q represent the real part of the in-plane complex wavevectors.

In order to excite SPPs in thin films it is necessary to couple the incoming light using, for example, a prism in the Kretschmann configuration. In this case, three media are involved: the entrance medium is a glass prism (n=1.5), the center medium is the RuO_2 film with a finite thickness d, and the exit medium is air (n=1) as shown in the inset in Fig. 4(b). In this configuration, a minimum in the reflected intensity is observed due to SPP excitation and absorption. Using a matrix transfer formalism to describe the light behavior in this multilayer system [31, 32], we computed the reflectance map of a RuO_2 thin film as a function of its thickness, the incident photon energy and the incidence angle. In the calculations, the incident light was considered p-polarized, the incident angle inside the glass prism was varied $\theta \in [0^\circ, 90^\circ]$, and the incident radiation energy was varied from 0.12 to 3eV spanning the region of interest. The simulated reflectance map for a 30 nm thick RuO_2 thin film using a Drude dielectric function is shown in Fig. 4(b). In the figure, high reflectance areas are shown in brighter contrast, while those with low reflectance due to absorptions appear darker. The dispersion relations curves shown in Fig. 4(a) can serve as guides to identify the different modes appearing in the reflectance map in Fig. 4(b). In Figs. 4(a) and 4(b), the region between the light lines in air and in glass refers to the angle region $\theta \in [\theta_c, 90^\circ]$ (where θ_c is the total internal reflection angle or critical angle), *i.e.* the region where leaky plasmon modes could be excited. In the lower left region in Fig. 4(b), between the light lines in air and in glass, a curved shaded region is observed corresponding to the SPP mode or Fano mode. The SPP excitation is very strong in the IR region and tends to vanish near ω_{sp}, which is consistent with the Fano dispersion curve. A second absorption band can be observed in the reflectance map corresponding to the bulk mode, which is much broader and extends from visible to IR. Remarkably SPPs and bulk polaritons overlap in the IR region. It is worth noticing that both bulk mode and SPP excitation depend strongly on the film thickness. In Fig. 4(b) we present the simulated reflectance map for a 30 nm thick film, *i.e.* the optimal thickness for SPP excitation. Nevertheless, for the bulk mode the strongest excitation in the visible red region is obtained for film thicknesses around 70 nm, as shown later. Thus, our calculations can be used to predict the behavior of films with different thicknesses.

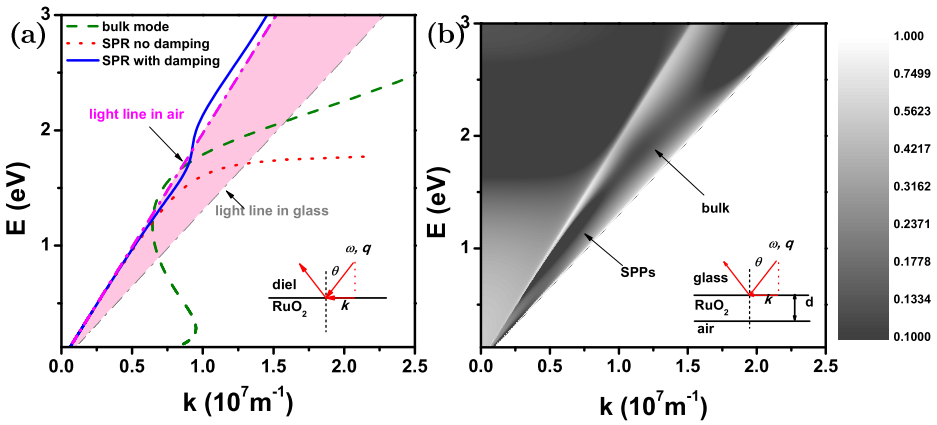

Fig. 4. (a) Dispersion relation curves corresponding to bulk and surface plasmon modes, as shown in Eqs. (1) and (2). A shadowed region is bounded by the light lines in air and in glass. Dispersion relations are plotted versus the real part of the in-plane wave vector k. (b) Simulated reflectance map for the three layer model with glass, 30 nm thick RuO_2 film and air. Light is incident from the glass side, in the domain $E \in [0.12eV, 3eV]$ - $\theta \in [0^\circ, 90^\circ]$. Reflectance in Fig. 4(b) is plotted in log scale to enhance picture contrast. High reflectance areas are shown as brighter, while low ones appear darker.

#162843 - $15.00 USD Received 9 Feb 2012; revised 22 Mar 2012; accepted 23 Mar 2012; published 28 Mar 2012

5. Results and discussion

In order to investigate the optical response of the RuO_2 thin films under plasmons excitation in the visible and IR regions we first used a cw *p*-polarized He-Ne red laser (λ = 632.8 nm) and a He-Ne IR laser (λ = 1520 nm). As discussed above, a strong excitation of SPPs is expected in the IR region, while the bulk mode is excited in both visible red and IR regions. Figure 5 shows both measured and simulated reflectance angular dependences in both the IR and the visible optical range for 30 nm RuO_2 thin films deposited on TiO_2 (001) (a, b) and glass substrates (c, d). The experimental and simulated reflectances for the TiO_2 and glass substrates alone are also shown for comparison. Interference oscillations found for the case of TiO_2 substrates were smoothed out for clarity. The experimental curves were normalized with respect to the intensity measured at $20°$, well below the critical angle θ_c. Figure 5 shows clear absorption of incoming light above the critical angle in the IR region, corresponding to SPP excitation, for both crystalline [RuO_2 on TiO_2 (001)] and polycrystalline [RuO_2 on glass] samples. A similar dip in the reflectance was also observed in the visible region, corresponding to bulk plasmon absorption. Comparatively, the SPP excitation measured in the IR region appeared much stronger than the bulk polaritons in the visible region in the 30 nm thick thin films. Comparing the experimentally measured and numerically simulated data we find better agreement between simulations and experimental measurements for crystalline RuO_2 films deposited on TiO_2 (001) substrates than for polycrystalline RuO_2 films deposited on glass substrates. Particularly, we note that the measured angle for maximum absorption agrees better with the simulation in the crystalline film due to lower concentration of structural defects. The simulations in Fig. 5(a) (solid line) clearly show excitation of both SPP (sharp absorption minimum near the critical angle) and of the bulk mode (broader dip at higher angle) [1]. The experimental results are not as sharp but still show convolution of two minima.

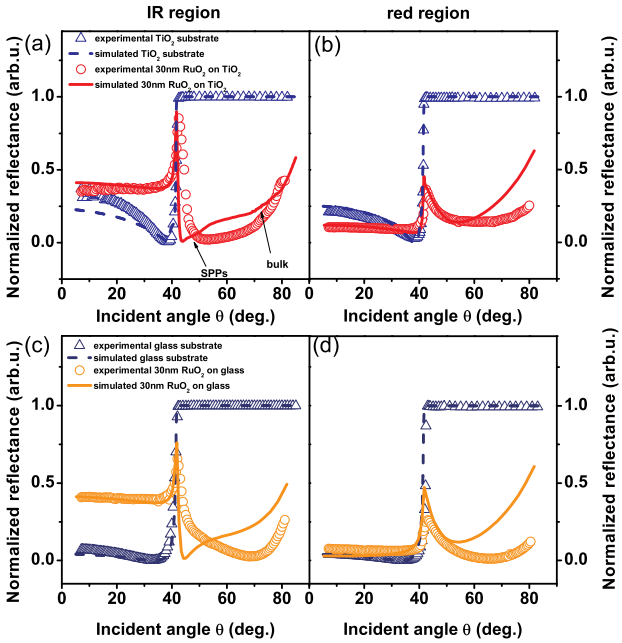

Fig. 5. Experimental (dots) and simulated (lines) angular reflectance dependence for 30 nm RuO_2 thin films deposited on TiO_2 (001) (a, b) and glass substrates (c, d) measured with IR and red laser. Experimental reflectance and simulation results of glass and TiO_2 (001) substrate are also included as comparisons. Better agreements between simulations and experimental measurements are obtained for the single crystalline RuO_2 on TiO_2 (001) compared to the polycrystalline RuO_2 on glass.

#162843 - $15.00 USD Received 9 Feb 2012; revised 22 Mar 2012; accepted 23 Mar 2012; published 28 Mar 2012

Since the RuO_2 films deposited on TiO_2 (001) substrate exhibit better agreement with simulations, the remaining sections will concentrate on investigating the SPPs in such films. Figure 6 shows the experimental angular reflectance dependence of Series I, *i.e.* 30 nm RuO_2 thin films deposited on TiO_2 (001) substrates at different O_2 partial pressures. While all the films exhibit a similar response, a clear trend is observed due to the different O_2 partial pressure used during growth. The RuO_2 film deposited at O_2 partial pressure of 0.04 mTorr, which was previously shown to have the structural and optical properties closest to bulk, also shows the strongest SPP excitation in the IR region, centered at an angle slightly higher than θ_c and convoluted with a broader bulk polariton absorption centered at a higher angle [Fig. 6(a)]. A similar trend is observed in the visible region, where only the bulk polariton absorption is observed [Fig. 6(b)].

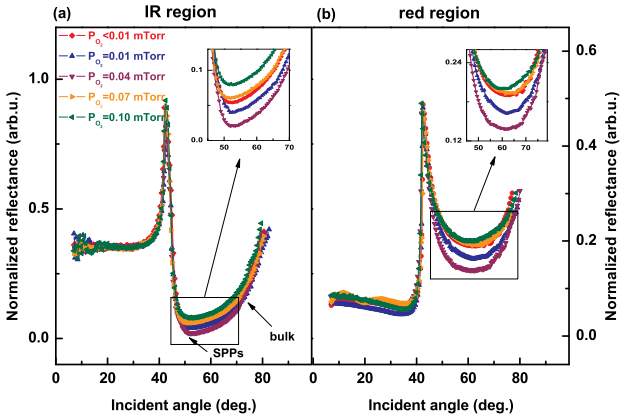

Fig. 6. Experimental angular dependence of the reflectance for Series I (30 nm RuO_2 thin films deposited on TiO_2 (001) substrates at different O_2 partial pressures) illuminated by IR laser (a) and red laser (b). RuO_2 deposited at O_2 partial pressure of 0.04 mTorr shows the strongest SPPs as well as bulk polaritons in the IR region and bulk polaritons in the visible red region.

We also investigated the effect of the thin film thickness in the excitation of the different polariton modes. Figure 7 shows angular dependence of the reflectance measurements for Series II, where RuO_2 thin films were deposited on TiO_2 (001) films with thickness of 17 nm, 30 nm, 73 nm and 128 nm at the optimized O_2 partial pressure. Normalized experimental reflectance curves for the Series II samples in the IR and visible red regions are shown in Figs. 7 (c), 7(d), and the corresponding simulations in Figs. 7 (c), 7(d). Our measurements indicate that bulk and surface polariton excitation strongly depend on thin film thickness in the different spectral regions: the highest overall absorption in the IR region due to both SPPs and bulk modes is observed for the 30-nm-thick film (Fig. 7(a)), while the optimum thickness for the bulk mode absorption is found for the 73-nm-thick film in the visible red region (Fig. 7(b)). Simulations (Figs. 7 (c), 7(d)) agree with the experimental data remarkably well. For the thinner film (17 nm, dashed light) simulations show a single minimum in the IR region (Fig. 7(c)) due to SPP excitation. For the 30 nm film (solid line) a very sharp minimum is observed immediately after the critical angle corresponding to SPPs convoluted with another broader minimum at higher angles corresponding to the bulk mode (as discussed for Fig. 5). These simultaneous SPPs and bulk modes can also be clearly observed in the 73 nm film (dash-dot line); showing the first minimum near the critical angle and the second minimum at a larger angle. For thicker films it is expected that the SPP mode decreases in intensity because most of the light is absorbed by the film and cannot reach the RuO_2/air interface to excite any SPPs. This is particularly noticeable for the 128 nm film (dash-dot-dot line), where SPPs appear significantly decreased, while the bulk mode shows a high absorption in the IR region.

#162843 - $15.00 USD Received 9 Feb 2012; revised 22 Mar 2012; accepted 23 Mar 2012; published 28 Mar 2012

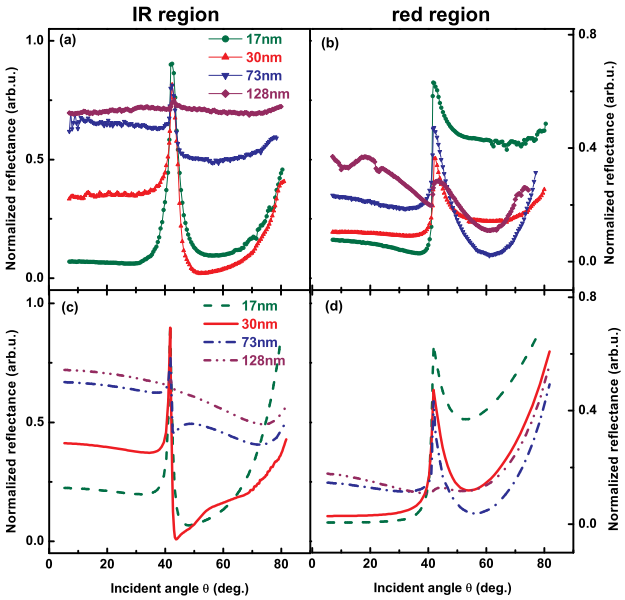

Fig. 7. Experimental angular dependence of the reflectance for Series II (RuO_2 thin films deposited on TiO_2 (001) substrates with O_2 partial pressure of 0.04 mTorr and different film thicknesses) illuminated by IR laser (a) and red laser (b), and corresponding simulation results (c, d). In the IR region, a 30 nm thick film shows the strongest absorption, while in the visible red region, a 73 nm thick film shows the strongest absorption. Simultaneous SPPs and bulk modes are observed in the IR region. Excellent agreement is achieved between experimental data and simulations.

In order to further investigate how the bulk and SPP modes evolve with photon energy, we mapped the evolution of the angular reflectance dependence for different wavelengths. Figure 8 shows the angular reflectance dependence for a 73 nm thick RuO_2 film on a TiO_2 (001) substrate (one of the samples in Series II) while varying the wavelength of the excitation laser from 800 to 1000 nm. For these measurements we used an 800 nm Coherent Legend femtosecond laser system with a TOPAS parametric amplifier, which produced approximately 100 fs pulses with power <100 μJ, at a widely tunable wavelength. These pulses were further attenuated and lengthened after passing through 7-meter multimode optical fiber. Figure 8 shows the experimental (a) and simulated (b) angular dependence of the reflectance at several different wavelengths from 800 nm to 1000 nm. While only the bulk mode is observed in the

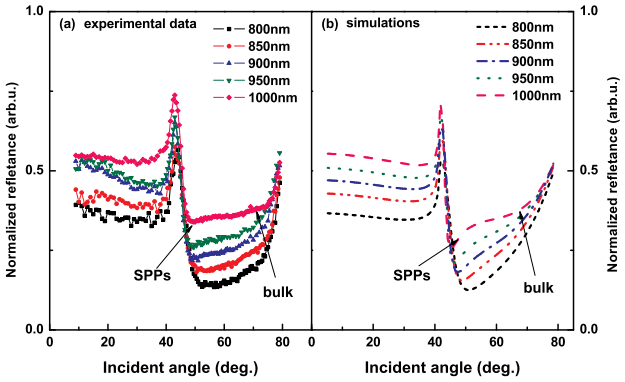

Fig. 8. Experimental (a) and simulated (b) angular dependence of the reflectance for a 73 nm RuO_2 thin film deposited on TiO_2 (001) substrate illuminated at different wavelengths ranging from 800 nm to 1000 nm. Only the bulk mode is observed in the visible region while simultaneous bulk and SPP modes are observed in the IR region.

#162843 - $15.00 USD Received 9 Feb 2012; revised 22 Mar 2012; accepted 23 Mar 2012; published 28 Mar 2012

visible-near IR region, the bulk mode becomes weaker and the SPP mode becomes clearer as the wavelength is increased towards the IR spectral region, in agreement with the previously shown results.

6. Conclusions

We have studied a potential alternative low-loss conductive oxide RuO_2 for the development of novel metamaterials and plasmonic applications. In the present work we report on the investigation of the SPPs and bulk polaritons in RuO_2 films. RuO_2 thin films were deposited by DC reactive magnetron sputtering on TiO_2 (001) and glass substrates. RuO_2 on TiO_2 (001) grown at an optimal O_2 partial pressure shows the best microstructure, electrical and optical properties. From optical measurements and simulations, SPPs and bulk polaritons were observed in the IR region while only bulk polaritons were detected in the visible red region. The experimental results on single crystalline RuO_2 deposited on TiO_2 (001) showed better agreement with the simulations than the polycrystalline RuO_2 on glass due to closer to bulk behavior in the former and increased defects in the latter. We found that the strength of SPPs and bulk polaritons highly depended on the film thickness and incident wavelength. The largest absorptions were observed on the 30 nm thick film in the IR region for the case of SPPs and on the 73 nm thick film in the visible red region for the bulk polariton modes. These studies illustrate the possibility of controlled tuning of polariton excitation in these conducting oxide films.

Acknowledgments

This work is financed by NSF, DMR-1006013: Plasmon Resonances and Metal Insulator Transitions in Highly Correlated Thin Film Systems. We also acknowledge support from the NRI/SRC sponsored ViNC center. We thank Norfolk State University for the use of the XRD facility at the Applied Research Center, Jefferson Lab.

#162843 - $15.00 USD Received 9 Feb 2012; revised 22 Mar 2012; accepted 23 Mar 2012; published 28 Mar 2012